Liquefaction potential and strain dependent dynamic properties of Kasai River sand

Rana Chattaraj *, Aniruddha Sengupta

Department of Civil Engineering, Indian Institute of Technology Kharagpur, Kharagpur 721302, India

ABSTRACT

The availability of efficient numerical techniques and high speed computation facilities for carrying out the nonlinear dynamic analysis of soil-structure interaction problems and the analysis of ground response due to earthquake loading increase the demand for proper estimation of dynamic properties of soil at small strain as well as at large strain levels. Accurate evaluation of strain dependent dynamic properties of soil such as shear modulus and damping characteristics along with the liquefaction potential are the most important criteria for the assessments of geotechnical problems involving dynamic loading. In this paper the results of resonant column tests and undrained cyclic triaxial tests are presented for Kasai River sand. A new correlation for dynamic shear damping (D_s) and maximum dynamic shear modulus (G_{max}) are proposed for the sand at small strain. The proposed relationships and the observed experimental data match quite well. The proposed relationships are also compared with the published relationships for other sands. The liquefaction potential of the sand is estimated at different relative densities and the damping characteristics at large strain level is also reported. An attempt has been made to correlate the G_{max} with the cyclic strength of the soil and also with the deviator stress (at 1% strain) from static triaxial tests.

© 2016 Elsevier Ltd. All rights reserved.

1. Introduction

A number of important structures including railway bridges, road bridges, embankments and other water retaining and intake/outlet structures are constructed over the Kasai River and with the rapid industrialization and increase in population in the area several more such structures have been proposed. The existing twin railway bridges which connect two important cities in the area, Midnapore and Kharagpur, located on either banks of the river in the state of West Bengal is shown in Fig. 1. The proximity of a number of faults, like Pingla fault, Garhmayna Khandaghosh Fault and Eocene Hinge Zone, to the Kasai River [7] has caused mild seismic shaking a number of times in the recent past. A magnitude of $M_w = 4.9$ was recorded at Kharagpur during the 06/02/2008 Earthquake [23]. The area under consideration comes under the Seismic Zone III in the seismic zonation map of India. The Peak Ground Acceleration (PGA) predicted by GSHAP Model [16] for the area is between 0.2–0.3 g. Thus the seismic vulnerability assessment of the structures located on Kasai River is very much required to minimise the potential loss during a seismic event. The dynamic analysis of buried structures, embankments and foundations structures require that the constitutive relationships for the soils or the foundation soils be known a priory. A number of advanced constitutive relationships like that by Prevost [21], Dafalias et al. [6], Lade [19], Yang et al. [35], Elgamal et al. [10] and others are existing for this purpose. However, these advanced constitutive relationships for soils require extensive experience or knowledge regarding them and regarding their implementation in a software package. The most of the commercial analytical software for the dynamic analysis of soils/foundation soils require one to define the curves for the modulus degradation with strain and development of damping ratio with strain for the soils under consideration. These set of curves are popularly known as 'back bone curves'. These two curves are obtained from the laboratory dynamic tests on the soils and they incorporate the inelastic and nonlinear behaviors of a soil with the increment of strains. They are relatively easy to implement in a software due to their simplicity and thus they are more popular among the practicing engineers than the other more sophisticated models for the soils. In the literature, such sets of curves are available for sands [28], clays [33] and other materials.

In this research work, these back bone curves are developed for a local sand known as Kasai River sand. Often practicing engineers, instead of developing these curves from the laboratory tests on the specific soil, choose a set of curves from the literature. The set of

Nomenclature

|			
B	Pore pressure parameter	Δu	Change in sample pore pressure
CSR	Cyclic stress ratio	V_s	Shear wave velocity
D_s	Dynamic shear damping	Pa	Atmospheric pressure
e	Void ratio	$\Delta\sigma_c$	change in cell pressure
G	Shear modulus	ρ	Density of the soil specimen
G_{max}	Maximum dynamic shear modulus	τ	Shear stress
N	Number of cycles	γ	Shear strain
r_u	Pore water pressure ratio	σ_0	Effective confining pressure
		σ_d	Deviator stress
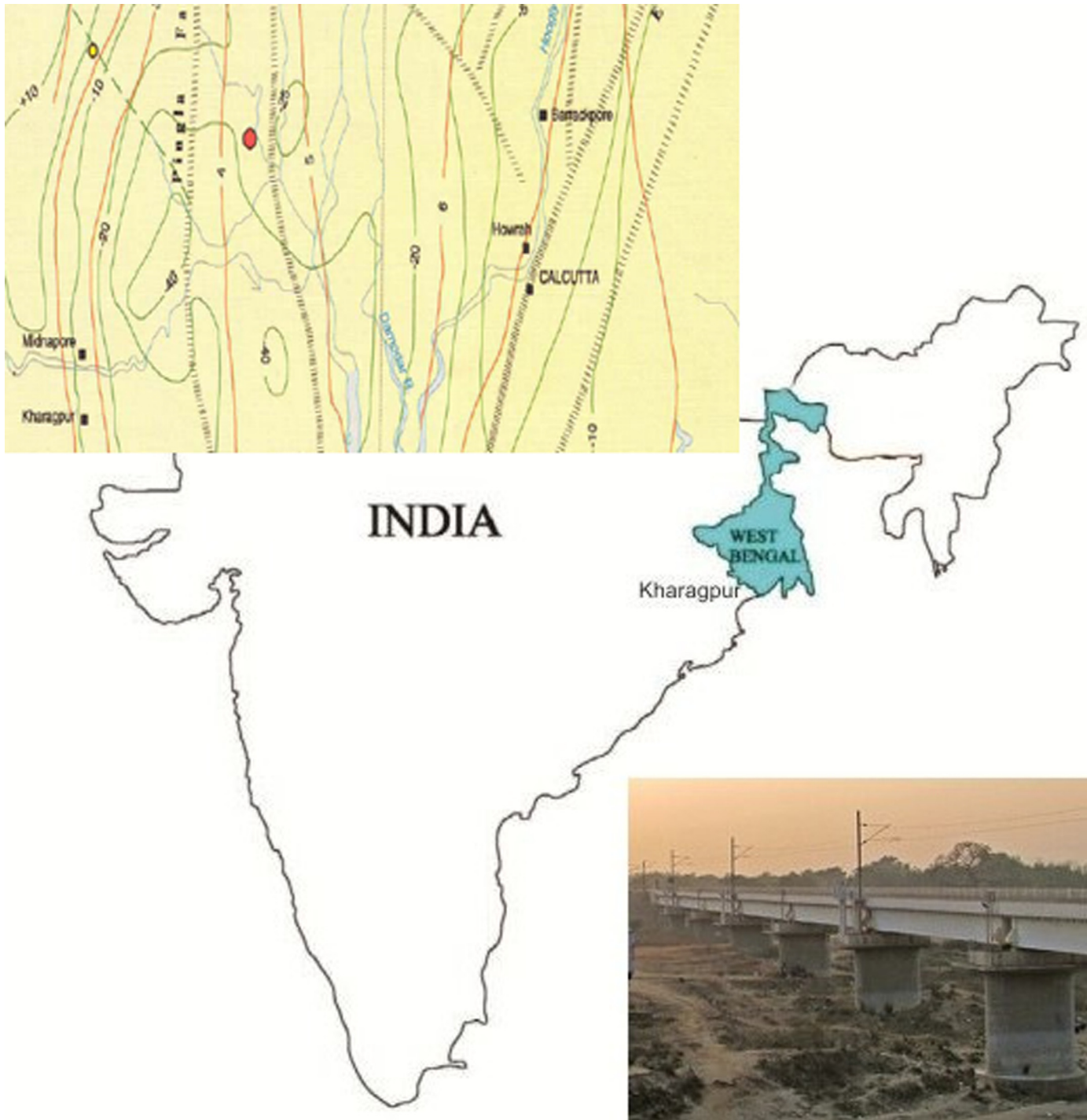
Fig. 1. Twin rail bridges connecting Kharagpur and Midnapore.

curves as well as the liquefaction curve developed for the Kasai River sand in this study are compared with the published curves on other sands. It is demonstrated in this research work that these back bone curves vary from sand to sand based on their grain size distribution and other characteristics. The results from this study may be readily used to analyze foundations located on sands with similar characteristics as the Kasai River sand.

Small strain as well as large strain dependent dynamic properties of the sand subjected to dynamic loading has been investigated extensively by various researchers by means of resonant column test and dynamic triaxial test. Hardin [13] has given a formula for estimation of G_{max} for sand and clay. Chung et al. (1986) has conducted resonant column test on solid and hallow cylindrical specimens of Monterey sand 0 to study the small strain dynamic properties of the sand. Saxena and Reddy [27] have also performed the resonant column tests on Monterey sand 0 and proposed new relationships for the dynamic shear modulus and the dynamic longitudinal modulus along with the damping. Based on the laboratory tests and field tests, Seed et al. [28] have given a simple relationship for the estimation of G_{max} and also reported modulus reduction curve with strain. Ishihara et al. [18] and Saxena et al. [26] have extensively studied the undrained cyclic strength of the sands by cyclic triaxial test. De Alba, et al. [9], Tokimatsu and Uchida [32] and Chen et al. (2005) have given correlation between the liquefaction potential of a soil and the shear wave velocity. The effect of percentage of silt on the liquefaction resistance of a silty sand is extensively studied by Erten and Maher [11], Polito and Martin (2001) [4], Xenaki and Athanasopoulos [34] and by Dash and Sitharam [8]. The effect of plasticity on cyclic behavior of soil is studied by Vucetic and Dobry [33]. SPT based liquefaction triggering procedure had been proposed by many researchers, such as Seed et al. [29], Idriss and Boulanger [15]. CPT based liquefaction triggering procedure was proposed by Moss et al. [20], Idriss and Boulanger [14] and Boulanger et al. (2015). CPT and SPT based liquefaction triggering procedure and their correlation was proposed by Boulanger and Idriss [24]. Some of the published relationships on sand are well established but may not hold for all sands and they need to be verified for a sand and/or alternative relationships should be developed for use in the subsequent dynamic analysis. In this particular study this is done for the Kansai River sand.

2. Soil properties and characterization

The index properties of the Kasai River sand are determined from the laboratory tests and presented in Table 1. The grain size distribution curve for the sand is given in Fig. 2. The Kasai River
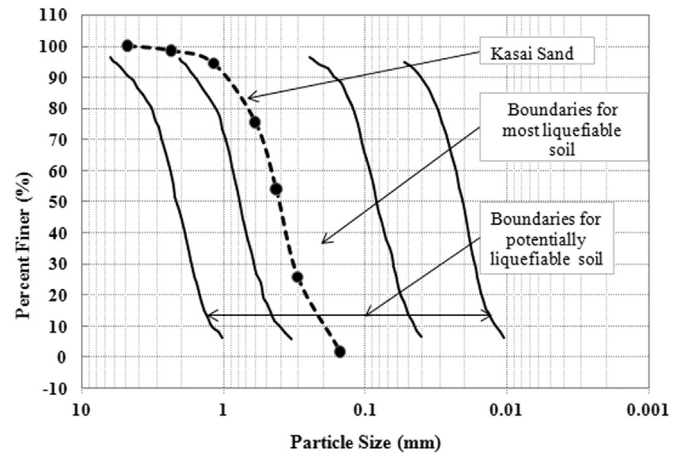
Table 1
Index properties of the Kasai River sand.

Index Property	Value
Specific Gravity	2.64
Coarse Sand (%)	1.7
Medium Sand (%)	44.0
Fine Sand (%)	54.0
Fine Content (%)	0.3
Maximum Void Ratio (e_{max})	0.83
Minimum Void Ratio (e_{min})	0.56
D_{10}	0.20
D_{30}	0.32
D_{60}	0.47
Coefficient of Uniformity (C_u)	2.36
Coefficient of Curvature (C_c)	1.08
Angularity	0.82
Sphericity (ψ)	0.78

Fig. 2. Particle size distribution curve superimposed with Liquefiable boundary.

sand is classified as poorly graded sand (SP) according to the Unified Soil Classification System [2]. The range of the grain size distribution of the most liquefiable soils and potentially liquefiable soils as proposed by Tsuchida (Xenaki-2003) are also shown in Fig. 2. As may be seen from this figure, the liquefaction potential of the sand is high.

3. Sample preparation

A split mould with 70 mm internal diameter and 140 mm height is used to prepare the test samples. All the samples are prepared by tamping method as per ASTM D 5311-11 [1] guidelines in three layers with oven dried soil. A funnel with a long tube is used in pouring the soil into the mould. The funnel is raised slowly during the process to maintain zero dropping height of the soil. Depending on the relative density of the sample to be tested, the required amount of sand is calculated for each layer of fill in the mould. After placing the sand into the mould, tamping is applied till it occupies one third height of the mould. The same technique is used to prepare the second and the third layers. Sitharam et al. [30] has shown that the in-situ soil fabric structure of the river sand can be recreated in the laboratory by using dry pluviation technique. Before removing the soil sample from the split mould, a small amount of suction (10–12 kPa) is applied to the specimen. Suction makes the sample stiff and consequently disturbance to the sample is reduced while removing the split mould and transferring the soil sample to the triaxial cell. The soil sample is prepared at four different target relative density (RD) of 25, 40, 60% and 80%.

4. Test procedure

4.1. Resonant column test

A fixed-free type resonant column device is used in this study. As the dynamic properties of sand do not differ significantly in saturated and dry conditions (Saxena et al., 1989), all the resonant column tests are conducted in dry condition on 70 mm diameter and 140 mm high soil samples. An all around confining pressure is applied to the sample inside the latex membrane by filling the chamber between the outer cover and the soil sample with water. Tests are conducted at four different effective confining pressures (σ_0) of 50, 100, 200 and 400 kPa. To prevent leakage into the sample, the latex membrane surrounding the soil sample is securely attached to the bottom pedestal and top cap with o-rings.

The torque is applied to the soil specimen by a system which essentially consists of four magnets. After applying the required confining pressure to the soil sample, a small amount of electric current (0.001–0.005 V) is passed through the magnetic coils with frequency ranges between 30 and 250 Hz with an increment of 5 Hz to excite the soil sample. This process is called broad sweeping. After roughly fixing the fundamental mode of vibration, a finer sweep is carried out with ± 5 Hz on either side of the fundamental mode of frequency with an increment of 0.2 Hz to find out the resonant frequency of the system and the corresponding strain within the soil sample. Later on the voltage is increased incrementally and for each increment of voltage, the above mentioned process is repeated. This procedure is terminated when the strain in the sample is more than 0.01%. For all the resonant column tests, the reference strain is taken as 0.001%. The reference strain is defined as a strain below which the shear modulus of the soil is assumed to be constant. For the resonant column tests, sample with relative density (RD) of 25, 40, 60% and 80% is considered.

4.2. Cyclic triaxial test

After the preparation of the soil sample, back pressure in the sample is applied to saturate the sample by using de-aired water while keeping the cell pressure 20–25 kPa higher than the back pressure. This process is terminated when the pore pressure parameter B ($B = \Delta u / \Delta \sigma_c$, where, Δu = change in sample pore pressure, and $\Delta \sigma_c$ = change in cell pressure) exceeds 0.95. After saturation, the sample is allowed to consolidate to an isotropic effective confining pressure of 100 kPa. After completion of the consolidation process, a constant cyclic stress ratio (CSR) of varying magnitude is applied to the sample. The cyclic stress ratio of 0.13, 0.18 and 0.23 are applied to the soil samples of 25% and 40% relative density and CSR of 0.13, 0.23 and 0.33 are applied to the soil samples of 60% and 80% relative density. A sinusoidal harmonic loading of a frequency of 1 Hz is applied for the entire test program. All the specimens are cyclically loaded until the occurrence of initial liquefaction (when the ratio of the excess pore pressure to the effective confining pressure becomes one). A built-in data acquisition system is used to monitor sample pore water pressure, cell pressure, axial deformation and cyclic loading during a test.

5. Results and discussion

5.1. Effect of confining pressure on the shear modulus at small strain

Fig. 3 illustrates the effect of confining pressure on the variation of shear modulus with strain for the Kasai River sand at a relative
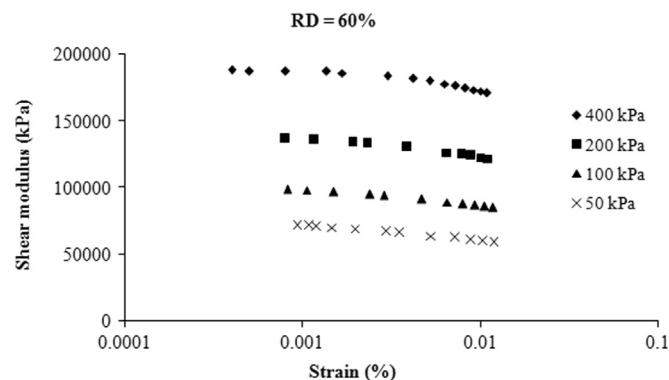
Fig. 3. Effect of confining pressure on the variation of shear modulus with strain for RD=60%.
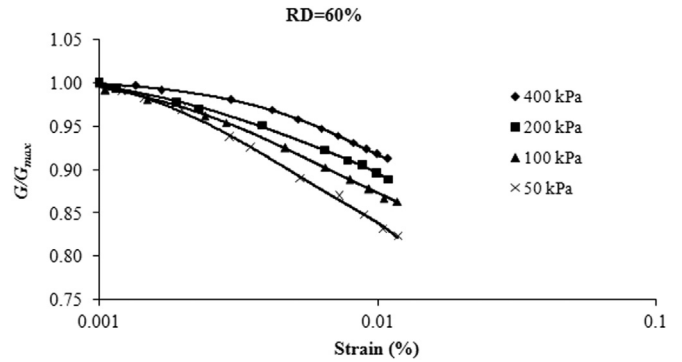
Fig. 4. Modulus reduction curve with strain for RD=60%.

density of 60%. From the figure, it is evident that at a given confining pressure, the shear modulus (G) decreases as the strain increases. It is also evident that at a given relative density, G_{max} decreases as the confining pressure decreases. At any strain level and relative density, the shear modulus is higher for a higher confining pressure. It is also observed that at the strain level less than 0.001%, the shear modulus is not changing significantly. Thus the shear modulus corresponding to the 0.001% strain is treated as the maximum dynamic shear modulus (G_{max}). The modulus reduction curves of the soil with effective confining pressure for relative density 60% are given in Fig. 4. From the figure, it may be seen that at a given relative density, the rate of reduction of G/G_{max} increases as the confining pressure decreases. Similar findings are also reported by Ishibashi [17].

5.2. Effect of relative density on shear modulus at small strain

It was observed that, at a given confining pressure, the shear modulus decreases as the relative density decreases. It was also observed that, at higher confining pressure, G/G_{max} does not vary significantly with the relative density, while at low confining pressure, G/G_{max} is considerably dependent on the relative density. At a low confining pressure, the soil at a low relatively density losses its shear strength at a faster rate than the soil at a higher relative density. At a strain level of 0.01% and 400 kPa confining pressure, the soil at 80% and 25% relative densities lose their shear strength approximately by 8.5% and 9.5%, where as at the same strain level and 50 kPa confining pressure, the losses in the shear strengths are 14% and 19%, respectively.

5.3. Correlating G_{max}, σ_0, and void ratio (e) at small strain

A number of empirical relationships between G_{max}, e and σ_0 exist in the literature. The relationships proposed by the Hardin [13], Chung et al. [5] and Saxena et al. (1989) are given below:

$$G_{max} = \frac{625 \times (Pa)^{0.5} \times (\sigma_0)^{0.5}}{(0.3 + 0.7e^2)} \tag{1}$$

$$G_{max} = \frac{523 \times (Pa)^{0.52} \times (\sigma_0)^{0.48}}{(0.3 + 0.7e^2)} \tag{2}$$

$$G_{max} = \frac{428.2 \times (Pa)^{0.426} \times (\sigma_0)^{0.574}}{(0.3 + 0.7e^2)} \tag{3}$$

Where, Pa is the atmospheric pressure. The unit of Pa is same as that of the confining pressure, σ_0, in the above equations.

Based on the present test data on the Kasai River sand, the
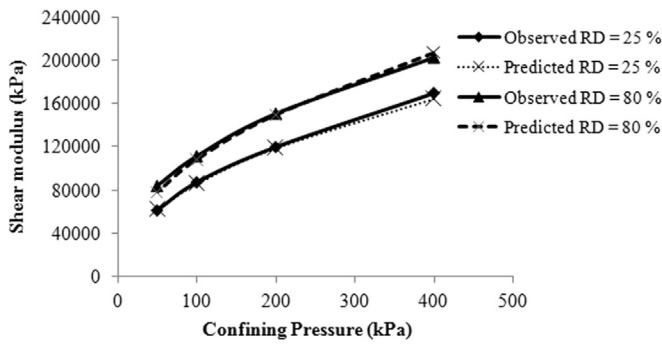
Fig. 5. Observed and predicted G_{max} at RD = 25% and 80%.

following empirical relationship is developed.

$$G_{max} = \frac{611.58 \times (Pa)^{0.532} \times (\sigma_0)^{0.468}}{(0.3 + 0.7e^2)} \tag{4}$$

As the above equation is dimensionally correct, this equation may be used in any system of units. The void ratio function $1/(0.3+0.7e^2)$ as proposed by Hardin [13] is adopted in the above relationship. Fig. 5 show the comparison between the test results and the prediction using Eq. (4) at different confining pressure and void ratio. It may be seen that the proposed relationship closely approximate the test data. Thus the proposed relationship may be used for the estimation of G_{max} of Kasai River sand for all practical purposes. Fig. 6 compares G_{max} obtained from the proposed relationship (Eq. (4)) with that obtained from the other empirical relationships ((Eqs. (1)–3)) at different confining pressures and void ratios. As the G_{max} depends on a number of factors such as soil type, grain size, void ratio, confining pressure, strain amplitude, sample preparation technique, testing equipment and technique, data interpretation, etc, the coefficients of the equation differ from sand to sand. It may be seen that the proposed relationship predicts G_{max} close to that by Hardin [13].

5.4. Effect of confining pressure and relative density on dynamic damping ratio at small strain

Based on the regression analysis of the experimental results the following expression is proposed for the dynamic damping ratio, D_s.

$$D_s = 41.17 \left(\frac{\sigma_0}{Pa}\right)^{-0.28} (\gamma)^{0.715} \tag{5}$$

where, γ is the dynamic shear strain, Pa is the atmospheric pressure and σ_0 is the effective confining pressure. The values of σ_0 and
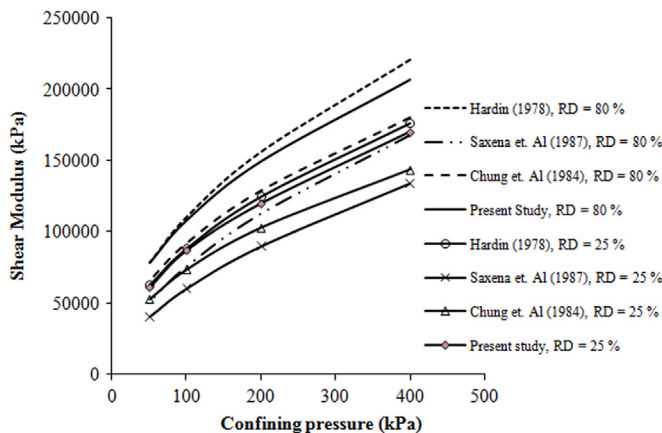

Fig. 6. Predicted G_{max} and Reported G_{max} by other author for RD = 25% and 80%.
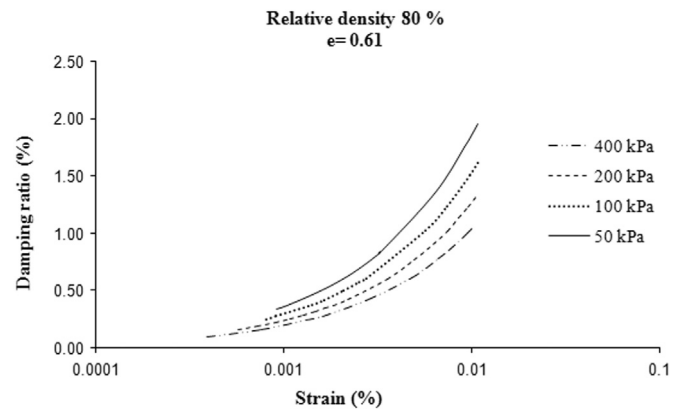

Fig. 7. Variation of damping ratio with strain for RD=80%.

Pa are in the same units and D_s and γ are in percentage. The above expression is non-dimensional and may be used for any system of units. The dynamic damping ratio at low strain is highly dependent on strain level and confining pressure. Fig. 7 show the variation of the damping ratio with the effective confining pressure. It is evident from the figure that at a constant void ratio, the damping ratio increases with the decrease in the confining pressure. Similar finding is reported in the literature (Saxena et al.,1989; [36]). It was also observed that the effect of relative density on the damping ratio is not significant. Similar observations are reported by Hardin [12], Tatsuoka (1978), and Saxena et al. (1989).

5.5. Comparison between reported and proposed empirical relationships for D_s

The accurate estimation of the damping ratio is extremely difficult when the magnitude of the damping ratio is less than 1% [5]. The empirical relationship for the dynamic damping ratio proposed by Saxena et al. (1989) is given below:

$$D_s = 9.22 \left(\frac{\sigma_0}{Pa}\right)^{-0.38} \gamma^{0.33} \tag{6}$$

Fig. 8 compares the dynamic damping ratio predicted from the empirical relationship proposed by Saxena, et al. (1989) and Eq. (5) proposed here. It may be seen that the values of the dynamic damping ratio from the proposed equation differ from the values obtained from Saxena et al. (1989) at smaller strain but as the strain increases, the difference between the two predictions decreases.
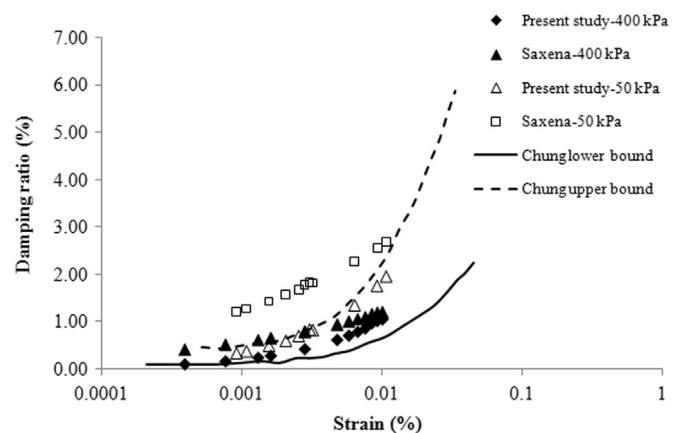

Fig. 8. Comparison of shear damping at 50 and 400 kPa.
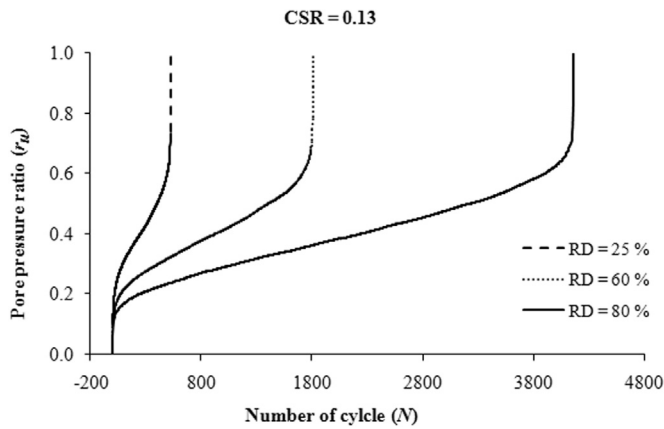
Fig. 9. Variation of pore pressure ratio with cycle ratio at different density.

5.6. Generation of excess pore water pressure due to cyclic loading

Fig. 9 illustrate the generation of pore water pressure with the number of loading cycle in the Kasai River sand at CSR of 0.13 and relative density of 25%, 60% and 80%. It may be seen from the figure that the pore water pressure increases with the increase in number of cycle and eventually it becomes equal to the initial effective confining pressure. At this stage, the effective stress in the sand becomes zero and initial liquefaction initiates. It may also be seen that at the initial few cycles, the pore water pressure generates at a faster rate and eventually it become stable with slower rate. But at the last few cycles, the pore water pressure shoots up rapidly due to the large shear deformation in the soil and leads to initialization of the liquefaction.

5.7. Effect of density on double amplitude axial strain

Fig. 10 depicts the effect of relative density on the variation of double amplitude axial strain with the number of cycles at a constant CSR of 0.13. From the figure it may be seen that the double amplitude axial strain at initial liquefaction is higher in the case of loose sand compared to the dense sand, which signifies that the loose sand deforms more during initiation of liquefaction. It may also be seen from the figure that for all samples, rapid shear deformation initiates during last few cycles of loading.

5.8. Cyclic strength of the soil and its correlation with G_{max}

Fig. 11 describes the cyclic resistance curve of the Kasai River sand at four different relative densities. The cyclic strength of the
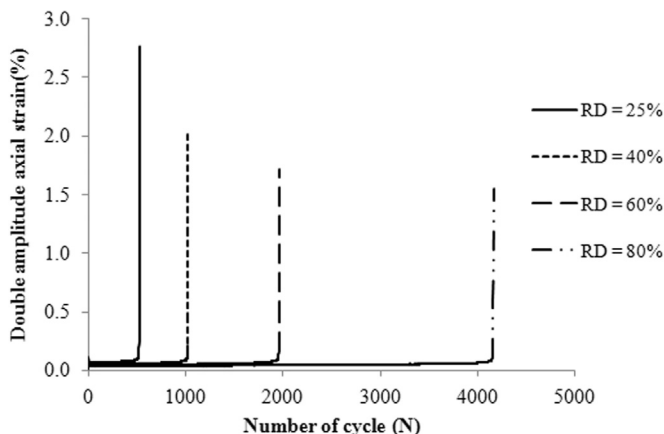

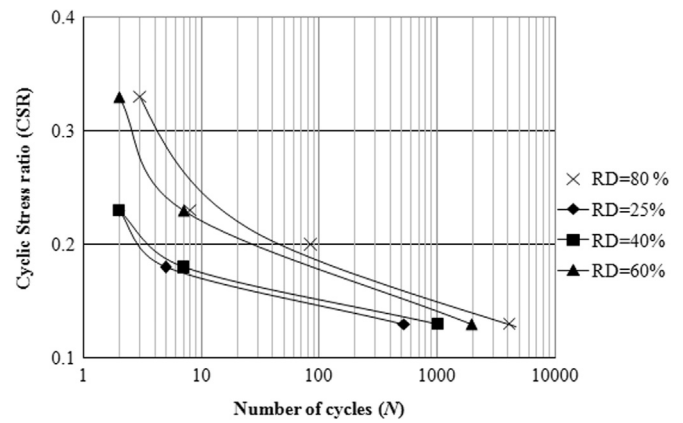Fig. 10. Variation of double amplitude axial strain with number of cycle for CSR = 0.13.

Fig. 11. Variation of cyclic stress ratio with number of cycle.

sand is defined as the stress ratio required for the initial liquefaction at a specified number of cycles. In this study, cyclic stress ratios required for initial liquefaction at 5, 10 and 20 cycles are found out and given in Table 2. It may be seen from Fig. 11 that the cyclic strength of the sand is greatly influenced by the relative density. The cyclic strength increases as the relative density increases. The cyclic stress ratio required for the initial liquefaction at 5, 10 and 20 cycles for RD = 80% is 1.57, 1.44 and 1.37 times higher than the sand at 25% relative density. It is also found that cyclic stress ratio required for initial liquefaction at 5 cycles at RD = 25% is 1.11 times higher than the stress ratio required for initial liquefaction at 20 cycles. It is 1.27 times higher in the sample at 80% relative density.

The variation of cyclic stress ratio (CSR) with number of cycle which causes the initial liquefaction (N_L) can be expressed in the following form (Saxena et al.,1987), Boulanger and Idriss [24].

$$CSR = a(N_L)^{-b} \tag{7}$$

Where 'a' and 'b' are constants which depend on the density of the sand. The values of 'a' and 'b' obtained from the experimental results, are reported in Table 3 along with those suggested by Rad and Clough [22]. Previous investigators found that the cyclic shear strength and dynamic moduli (or shear wave velocity) are influenced by some common factor such as density, stress history, strain, soil structure etc. Thus a correlation between dynamic moduli and cyclic shear strength makes sense. To develop the correlation, De Alba et al. [9] took a cyclic stress ratio (CSR) which causes initial liquefaction in 10 cycles as the cyclic shear strength, whereas Tokimatsu et al. [31] reported a CSR which causes initial liquefaction in 20 cycles as the cyclic shear strength of the soil. In this study CSR causing initial liquefaction at 5, 10 and 20 cycles of loading is utilized for the correlation. To develop the correlation, results from resonant column tests as well as cyclic triaxial tests are utilized. The maximum shear modulus (G_{max}) is calculated using Eq. (4), which is suggested for the resonant column test in this study. The relation between G_{max} and stress ratio required to cause initial liquefaction in 10 cycles has been shown in Fig. 12. It

Table 2
CSR required for initial liquefaction at 5, 10 and 15 cycles.

Relative density	Cyclic strength at initial liquefaction		
	5 cycles	10 cycles	20 cycles
25	0.18	0.17	0.162
40	0.186	0.175	0.167
60	0.24	0.22	0.205
80	0.283	0.245	0.223

Table 3
Values for the coefficients 'a' and 'b'.

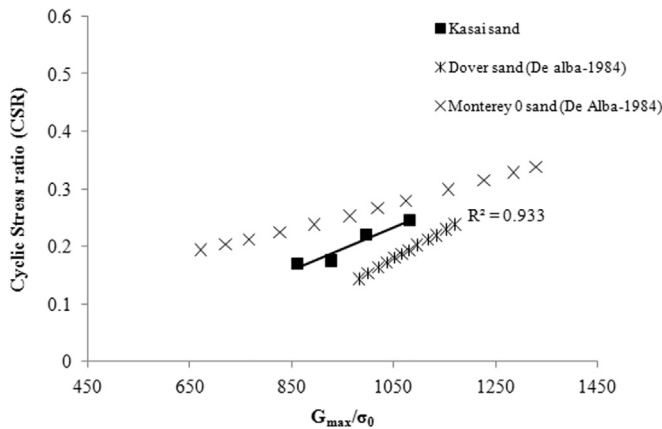| Relative density (%)	CSR = a $(N_L)^{-b}$		Relative density (%)	CSR = a $(N_L)^{-b}$	
	Present Study			Rad and Clough [26]	
	a	b		a	b
25	0.203	0.076	27	0.17	0.14
40	0.210	0.078	50	0.28	0.145
60	0.287	0.113	82	0.55	0.29
80	0.370	0.172			

Fig. 12. Variation of cyclic resistance with dynamic shear modulus for $N_L = 10$ cycles.
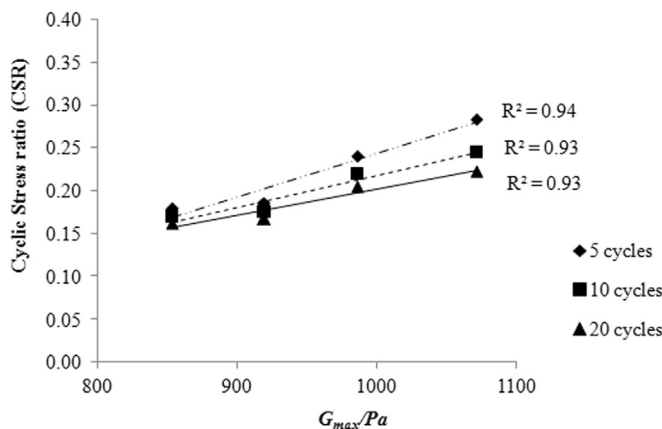

Fig. 13. Effect of specific number of cycle to cause liquefaction on the correlation between Maximum shear modulus and cyclic resistance of sand.

may be seen from the figure that a good correlation exists between the G_{max} and cyclic strength of the soil. The correlation for Monterey No.0 sand and Dover sand as reported by De Alba et al. [9] is also shown in Fig. 12. It may be also noted that De Alba et al. [9] have given the correlation in terms shear wave velocity. This shear wave velocity is used to calculate the G_{max} by taking the average unit weight of 15.3kN/m³ (97.6 pcf) for Monterey No 0 sand and 14.6 kN/m³ (93.15 pcf) for Dover sand. According to Saxena et al. (1987) the correlation between cyclic strength of the soil and G_{max} is material dependent and it is different for the different kind of material. Similar kind of finding is also reported by De Alba et al. [9] based on the laboratory tests on sand which are collected from different origin. Fig. 13 shows the effect of a particular number of cycles to initial liquefaction (N_L) on the correlation between cyclic strength of the soil and maximum shear modulus G_{max}. A high value of correlation coefficient indicates that there exists a good

correlation between dynamic moduli and cyclic shear strength for any N_L.

5.9. Correlation with static triaxial test results

The conventional static triaxial compression test is commonly used for soil testing as it is cost effective and easy to handle. On the other hand, the resonant column test is costly, uncommon and the test procedure is complicated. An effort has been made to correlate the maximum shear modulus obtained from the resonant column tests with the results obtain from the conventional static triaxial compression tests. It is felt that this kind of correlation will be useful to the practicing engineer for crude estimation of maximum dynamic shear modulus at the initial planning stage of a project. The consolidated undrained static triaxial tests are conducted on the dry Kasai River sand at 50, 100 and 200 kPa considering four relative densities of 25, 40, 60% and 80%. Chiang and Chae (1972) conducted undrained triaxial compression test and resonant column test at a confining pressure of 137.9kN/m² (20 psi) and have given the following correlation between maximum dynamic shear modulus and deviator stress correspond to 1% longitudinal strain obtained from the triaxial compression test

$$G_m = 13.867 + 0.419\sigma_d \qquad (8)$$

Where σ_d is the deviator stress corresponding to the 1% axial strain. Unit of the σ_d is in psi (1 psi = 6.89 kN/m²) and G_m is in ksi (1 ksi = 6.89 × 10³ kN/m²). To correlate the maximum dynamic shear modulus with the deviator stress at 1% of axial strain, Saxena and Reddy [25] proposed a similar kind of equation but in non dimensional form as shown below.

$$\frac{G_m}{P_a} = 1109.22\left(\frac{\sigma_d}{P_a}\right) + 72.47 \qquad (9)$$

The equation proposed by Saxena and Reddy is only applicable for a confining pressure of 49 kPa and is independent of relative density. Eqs. (8) and (9) do not consider the relative density and confining pressure. In the present study, an effort is made to consider the above parameters along with the deviator stress. The deviator stress corresponding to 1% axial strain from the triaxial tests is correlated to the maximum dynamic shear modulus obtained from the resonant column test by the following expression.

$$G_{max} = \frac{5219.58}{(0.3 + 0.7e^2)}(\sigma_0)^{0.426}(\sigma_d)^{0.088} \qquad (10)$$

Where σ_d is the deviator stress at 1% of strain from triaxial tests and σ_0 is the effective confining pressure. Instead of relative density, the void ratio function $1/(0.3 + 0.7e^2)$ is utilized. The value of the coefficient of determination (R^2) is found to be 0.99, which indicates the accuracy of the proposed correlation. It may be noted that the above relationship is valid within the range of 50 kPa and 200 kPa as all the static tests have been conducted within that range. Fig. 14 show the comparison between the measured G_{max} and the predicted G_{max} using Eq. (10) at different confining pressure and void ratio. It is observed that the proposed relationship very closely approximate the measured G_{max}. Thus the proposed relationship may be used for the estimation of G_{max} of Kasai River sand for all practical purposes.

5.10. Variation of damping ratio and shear modulus with strain

Fig. 15 shows the relationship between shear strain and damping ratio. It may be seen that all the test data fall within a narrow band which signifies that relative density does not have significant influence on the damping ratio of the soil. On the other
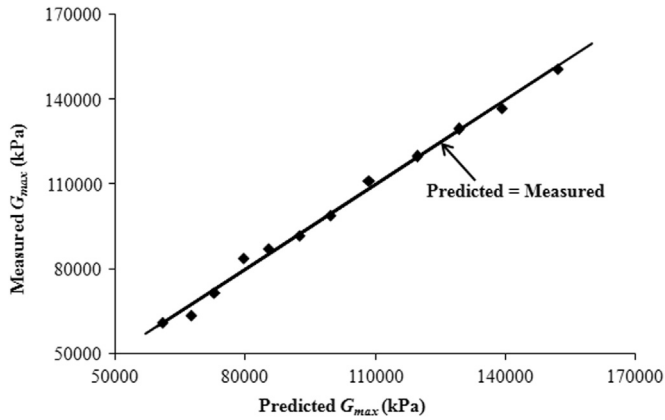
Fig. 14. Comparison of computed value of G_{max} form triaxial test with observed value of G_{max} in resonant column test for Kasai River sand.
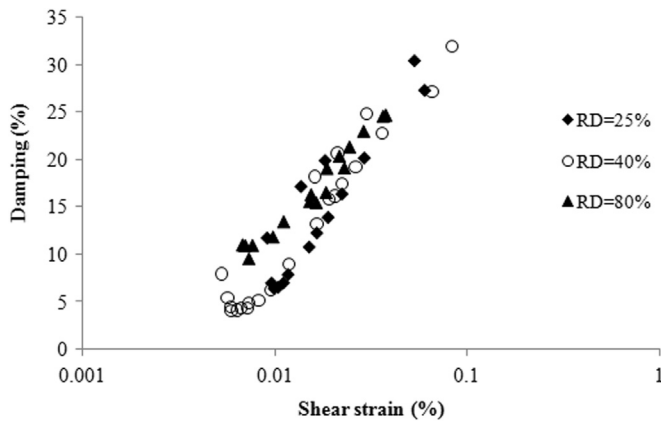

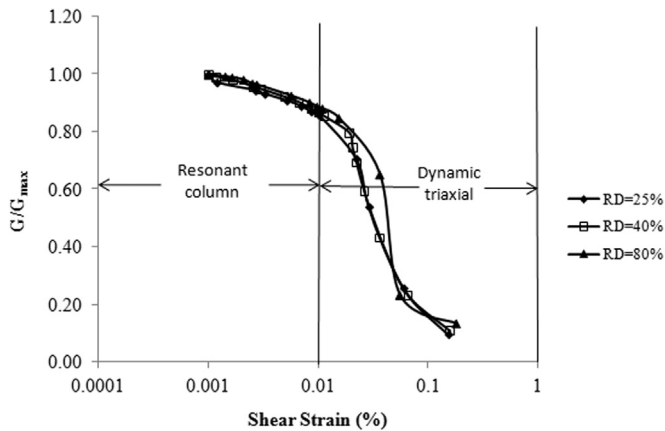**Fig. 15.** Variation of damping ratio with shear strain.

Fig. 16. Modulus degradation curve of the sand tested.

hand damping ratio increases significantly with the shear strain. Fig. 16 shows the modulus reduction curve for the Kasai River sand. In Fig. 16 G_{max} is calculated from Eq. (4) considering 100 kPa confining pressure as all the dynamic triaxial tests are conducted at 100 kPa confining pressure. The results from resonant column test as well as dynamic triaxial test at different strain level are shown in the above mentioned figure. For dynamic triaxial tests, the slope of the secant line corresponding to the tip of the loop is taken as shear modulus (G). It may be seen that within the range of 0.01% and 0.1% shear strain, the shear modulus degrades drastically due to rapid generation of excess pore water pressure.

6. Conclusions

Small strain dynamic properties and liquefaction potential of the Kasai River sand depends on various factor such as confining pressure, relative density, particle size distribution, particle shape, fine content, stress history, sample preparation technique in the laboratory, etc. Due to the above mentioned factors, the maximum shear modulus, damping ratio and the liquefaction potential differ from soil to soil and for this reason correlations developed for one sand may not be valid for other sands. In the present investigation, new correlations are proposed for the maximum shear modulus (G_{max}) and dynamic shear damping (D_s) and their validity is discussed. These proposed relationships may be used readily for the similar kind of soils which have the grain size distribution curve similar to that of the Kasai sand. A relationship for the cyclic stress ratio (CSR) causing initial liquefaction at different relative density is also developed and the coefficients of the equation are given in a tabular form for the ready use. A correlation between the maximum dynamic shear modulus with the cyclic stress ratio causing initial liquefaction at 5, 10 and 20 cycles has been developed to interpret the cyclic strength of the Kasai River sand from resonant column test results. For the crude estimation of G_{max} from the static triaxial tests, a correlation between the G_{max} and the deviator stress at 1% of axial strain is also proposed for the sand to help the practicing engineers. All the correlations proposed in this study are dimensionless and can be used for any system of units.

References

[1] ASTM Standard D-5311-11: Standard test method for load controlled cyclic triaxial strength of soil. West Conshohocken, Pennsylvania, USA: American Society of Testing and Materials.

[2] ASTM Standard D-2487-11: Standard practice for classification of soils for engineering purposes (Unified Soil Classification System). West Conshohocken, Pennsylvania, USA: American Society of Testing and Materials.

[4] Carmine PP, Martin II JR. Effects of nonplastic fines on the liquefaction resistance of sands. J Geotech Geoenviron Eng 2001;127(5):408–15.

[5] Chung RM, Yokel FY, Drnevich VP. Evaluation of dynamic properties of sand by resonant column testing. Geotech Test J GTJODJ 1984;7(2):60–9.

[6] Dafalias Y, Papadimitriou A, Li X. Sand plasticity model accounting for inherent fabric anisotropy. J Eng Mech 2004:1319–33. http://dx.doi.org/10.1061/(ASCE)0733-9399(2004)130:11(1319).

[7] Dasgupta S, Narula PL, Acharyya SK, Banerjee J. Seismotectonic Atlas of India and its environs. Kolkata, India: Geological Society of India; 2000.

[8] Dash HK, Sitharam TG. Undrained cyclic and monotonic strength of sand-silt mixtures. Geotech Geol Eng 2011;29(4):555–70.

[9] De Alba P, Baldwin K, Janoo V, Roe G, Celikkol B. Elastic-wave velocities and liquefaction potential. Geotech Test J GTJODJ 1984;7(2):77–87.

[10] Elgamal A, Yang Z, Parra E, Ragheb A. Modeling of cyclic mobility in saturated cohesionless soils. Int J Plast 2003;19(6):883–905 (Pergamon, Elsevier Science Ltd.).

[11] Erten D, Maher MH. Cyclic undrained behaviour of silty sand. Soil Dyn Earthq Eng 1995;14(2):115–23.

[12] Hardin BO. The nature of damping in sands. J Soil Mech Found Div 1965;91(1):63–95.

[13] Hardin, BO. The nature of stress-strain behaviour for soils. In: Proc. of Earthquake Engineering and Soil Dynamics. Pasadena, CA: ASCE; 1978:1:3-90.

[14] Idriss, IM, Boulanger, RW. Soil liquefaction during earthquakes. Monograph MNO-12. Oakland, CA: Earthquake Engineering Research Institute; 2008: 261 pp.

[15] Idriss IM, Boulanger RW. SPT-based liquefaction triggering procedures Davis, CA: Department of Civil and Environmental Engineering, University of California,; 2010 [Report UCD/CGM-10/02, 259 pp].

[16] IS 1893 (Part 1) 2002, Criteria for earthquake resistant design of structures. New Delhi: Bureau of Indian Standards, Govt of India; 2002.

[17] Ishibashi I. Discussion to "Effect of soil plasticity on cyclic response," by M. Vucetic and R. Dobry. J Geotech Eng 1992;118(5):830–2.

[18] Ishihara K, Tatsuoka F, Yasuda S. Undrained deformation and liquefaction of sand under cyclic stress. Soils Found 1975;15(1):29–44.

[19] Lade P. Overview of constitutive models for soils. Calibration Const Models 2005:1–34. http://dx.doi.org/10.1061/40786(165).

[20] Moss RES, Seed RB, Kayen RE, Stewart JP, Der Kiureghian A, Cetin KO. CPT-based probabilistic and deterministic assessment of in situ seismic soil liquefaction potential. J Geotech Geoenviron Eng 2006;132(8):1032–51 [ASCE].

[21] Prevost JH. A Simple Plasticity Theory for Frictional Cohesionless Soils. Soil Dyn Earthq Eng 1985;4(1):9–17.

[22] Rad NS, Clough WG. The influence of cementation on the static and dynamic behavior of sands Stanford, California: The John A. Blume Earthquake Engineering Center, Stanford Univ.; 1982 [Report No. 59].

[23] Raj A, Nath SK, Thingbaijam KKS. A note on the recent earthquakes in the Bengal basin. Curr Sci 2008;95(9):1127–9.

[24] Boulanger, RW, Idriss, IM. CPT and SPT based liquefaction triggering procedures. Davis, CA: Center for Geotechnical Modeling, Department of Civil and Environmental Engineering, University of California; 2014, Report No. UCD/CGM-14/01.

[25] Saxena, SK, Reddy, RK. Mechanical behavior of cemented sand. Chicago, IL: Report to the National Science Foundation, Department of Civil Engineering, Illinois institute of Technology; 1987, Report IIT-CE-8701.

[26] Saxena SK, Reddy KR, Avramidis AS. Liquefaction resistance of artificially cemented sand. J Geotech Eng 1988;114(12):1395–413.

[27] Saxena SK, Reddy KR. Dynamic moduli and damping ratio for Monterey No.0 sand by Resonant Column tests. Soils Found 1989;29(2):37–51.

[28] Seed HB, Robert TW, Idriss IM, Tokimats K. Moduli and damping factors for dynamic analyses of cohesionless soils. J Geotech Eng 1986;112(11):1016–32.

[29] Seed HB, Tokimatsu K, Harder Jr. LF, Chung R. Influence of SPT procedures in soil liquefaction resistance evaluations. J Geotech Eng 1985;111(12):1425–45.

[30] Sitharam TG, Govinda Raju L, Sridharan A. Dynamic properties and liquefaction potential of soils. Curr Sci 2004;87(10):1370–8.

[31] Tokimatsu K, Yamazaki T, Yoshimi Y. Soil liquefaction evalua-tions by elastic shear moduli. Soils Found 1986;26(1):25–35.

[32] Tokimatsu K, Uchida A. Correlation between liquefaction resistance and shear wave velocity. Soils Found 1990;30(2):33–42.

[33] Vucetic M, Dobry R. Effect of soil plasticity on cyclic response. J Geotech Eng 1991;117(1):89–107.

[34] Xenaki VC, Athanasopoulos GA. Liquefaction resistance of sand-silt mixture: an experimental investigation of the effect of fines. Soil Dyn Earthq Eng 2003;23:183–94.

[35] Yang Z, Elgamal A, Parra E. A computational model for liquefaction and associated shear deformation. J Geotech Geoenviron Eng 2003;129(2) [ASCE].

[36] Zhang J, Andrus D, Juang C. Normalized shear modulus and material damping ratio relationships. J Geotech Geoenviron Eng 2005;131(4):453–64.

Further reading

[3] Bhatia SC, Kumar M, Ravi, Gupta HK. A probabilistic seismic hazard map of india and adjoining regions. Ann Geofis 1999;42(6):1153–64.